ARTICLE

Ultrafast Decay Dynamics of N-Ethylpyrrole Excited to the S_1 Electronic State: A Femtosecond Time-Resolved Photoelectron Imaging Study

Wen-peng Yuan[a,b†], Bai-hui Feng[b,c†], Dong-yuan Yang[b*], Yan-jun Min[b,c], Sheng-rui Yu[a*], Guo-rong Wu[b*], Xue-ming Yang[b]

a. Hangzhou Institute of Advanced Studies, Zhejiang Normal University, Hangzhou 311231, China
b. State Key Laboratory of Molecular Reaction Dynamics, Dalian Institute of Chemical Physics, Dalian 116023, China
c. University of Chinese Academy of Sciences, Beijing 100049, China

(Dated: Received on April 6, 2021; Accepted on May 7, 2021)

N-ethylpyrrole is one of ethyl-substituted derivatives of pyrrole and its excited-state decay dynamics has never been explored. In this work, we investigate ultrafast decay dynamics of N-ethylpyrrole excited to the S_1 electronic state using a femtosecond time-resolved photoelectron imaging method. Two pump wavelengths of 241.9 and 237.7 nm are employed. At 241.9 nm, three time constants, 5.0±0.7 ps, 66.4±15.6 ps and 1.3±0.1 ns, are derived. For 237.7 nm, two time constants of 2.1±0.1 ps and 13.1±1.2 ps are derived. We assign all these time constants to be associated with different vibrational states in the S_1 state. The possible decay mechanisms of different S_1 vibrational states are briefly discussed.

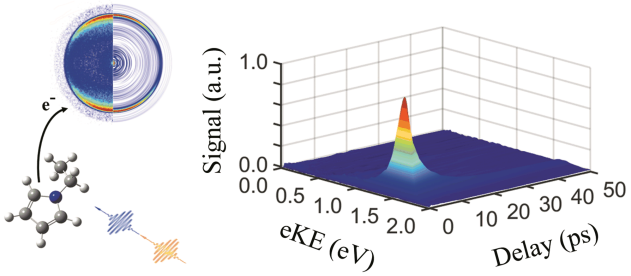

Key words: Photoelectron spectrum, Pump/probe, Femtosecond time-resolved

I. INTRODUCTION

Small isolated heteroaromatic molecules, such as pyrrole, imidazole, indole, *etc.*, offer ideal model systems for the understanding of electronic structure and photochemistry of a range of important biomolecules [1–4]. Among these prototypical heteroaromatic molecules, N-methylpyrrole ($C_4H_4NCH_3$) is one of methyl-substituted derivatives of pyrrole and contains an N-CH_3 group, which is a key building block in many biologically important complex molecules [5]. The UV absorption spectrum and the excited-state dynamics of N-methylpyrrole have been investigated in recent decades and the methyl substitution effects (compared to pyrrole) are explored and better understood [6–17]. In these studies, majority of the experimental and theoretical results could be rationalized within the framework proposed in the seminal theoretical studies by Domcke and coworkers [18, 19] and the role of the lowest-lying $^1\pi(3s/\sigma^*)$ state (predominantly 3s character in the Franck-Condon (FC) region and σ^* character at extended N−CH_3 bond length, hereafter termed simply as $^1\pi\sigma^*$) in the non-radiative decay of the excited states was confirmed.

For the bare pyrrole, the ultrafast dynamics of the $S_1(^1\pi\sigma^*)$ state with a lifetime of less than 50 fs at pump wavelengths of <250 nm [20–23] and 126 fs at 250 nm [21] has been previously reported. For the methyl-substituted derivatives of pyrrole, it could be generally classified into two categories: methyl-substitution in the ring C atom positions and methyl-substitution in N atom position. In the former case, methyl-substitution

†These authors contributed equally to this work.
*Authors to whom correspondence should be addressed. E-mail: yangdy@dicp.ac.cn, sryu@zjnu.cn, wugr@dicp.ac.cn

effects have limited influences on the decay dynamics of the S_1 state [24, 25], whereas in the latter case, it shows drastic differences in the lifetimes of the S_1 state. In particular, for methyl group substitution in N-position on pyrrole, *N*-methylpyrrole, it has a lifetime about one to three orders of magnitude longer than that of pyrrole depending on the vibrational excitation of the S_1 state [13, 14, 16], which was explained to be due to the change of the S_1 state potential energy surface with an increased barrier along the C−N dissociation coordinate [14]. In a recent picosecond pump-probe experiment by Kim and coworker, the lifetimes of the selective vibrational states in the S_1 state of *N*-methylpyrrole have been measured and show a general trend of decrease with the increase of vibrational energy [16]. However, it was also found to be strongly mode-dependent and a higher vibrational state may decay with a slower rate than a lower-energy one. Moreover, it is worth to note that dramatic decrease of the S_1 lifetime has been observed at $+806$ cm^{-1} above the S_1 origin.

In this work, we focus on an ethylated derivative of pyrrole, *N*-ethylpyrrole ($C_4H_4NCH_2CH_3$), and report a femtosecond time-resolved photoelectron imaging (fs-TRPEI) study of the ultrafast excited-state decay dynamics of *N*-ethylpyrrole. The motivations are similar to our previous studies on the ultrafast excited-state dynamics of several methyl-substituted derivatives of pyrrole, *N*-methylpyrrole (NMP) [13], 2,4-dimethylpyrrole (2,4-DMP) [24] and 2,5-dimethylpyrrole (2,5-DMP) [25]. We intend to understand the substitution effects on the excited-state dynamics of simple models, such as ethyl substitution in N-position on pyrrole herein, which may aid the development of simple models of such dynamics extendable to larger molecules. Unfortunately, studies on both electronic-state potential energy surfaces and the UV absorption spectrum of *N*-ethylpyrrole are very scarce, and its excited-state dynamics has not been explored both experimentally and theoretically. In the present work, the supersonic-jet-cooled *N*-ethylpyrrole molecules are excited by one-photon absorption at the pump wavelengths of 241.9 nm and 237.7 nm (5.13 eV and 5.22 eV), whereupon the delayed probe laser pulse of 280.8 nm (4.42 eV) produces photoelectrons via one-photon ionization. At these two pump wavelengths, the initial photoexcited state is attributed to vibrational excitation in the $S_1(^1\pi\sigma^*)$ state based on the analysis of time-resolved photoelectron spectra (TRPES) and the photoelectron angular distributions (PADs) and its decay dynamics is discussed in detail, compared with those of pyrrole and NMP.

II. EXPERIMENTS

The *N*-ethylpyrrole sample was obtained commercially (Macklin, ≥97%) and used without further purification. The UV absorption spectrum of *N*-ethylpyrrole under saturated vapor condition was measured at room temperature using a commercial UV-visible spectrometer (Shimadzu, UV-2600). The TRPEI experiment was carried out in a similar way to that previously described in our publications [24, 25], on a velocity map imaging (VMI) spectrometer [26]. The pump and probe laser pulses were obtained from a fully integrated Ti:Sapphire oscillator/regenerative amplifier system (<50 fs, 800 nm, 3.8 mJ and 1 kHz, Coherent, Libra-HE), followed by two commercial optical parametric amplifiers (OPA, Coherent, OPerA Solo), each was pumped by a fraction (1.3 mJ per pulse) of the fundamental output of the amplifier. The pump laser pulses of 241.9 and 237.7 nm (0.3−0.5 μJ per pulse) were directly obtained from one of the OPAs and the probe laser pulse of 280.8 nm (∼0.9 μJ per pulse) was obtained from the other OPA. The bandwidth of the pump laser pulses (full width at half maximum (FWHM) of the spectrum) of 241.9 and 237.7 nm was ∼270 cm^{-1} and ∼250 cm^{-1}, respectively, and ∼230 cm^{-1} for the probe laser pulse of 280.8 nm.

The seeded *N*-ethylpyrrole molecular beam was generated by bubbling 2 bar of helium carrier gas through a liquid sample at room temperature using an Even-Lavie pulse valve (200 μm diameter nozzle orifice) operated at 1 kHz and expanded supersonically into a high vacuum source chamber. Then the molecular beam entered into the interaction chamber of the VMI spectrometer through a 1 mm skimmer (Beam Dynamics Inc., Model 1) which was about 40 mm downstream of the nozzle. The pump and probe laser pulses were combined collinearly on a dichroic mirror without further compression, and then focused using an f/75 lens into the interaction region of the VMI spectrometer to intersect the seeded *N*-ethylpyrrole molecular beam. Both the pump and probe laser pulses were linearly polarized and the polarization direction was parallel to the micro channel plate (MCP) detector of the VMI spectrometer. A computer-controlled linear translation stage (Newport, M-ILS250HA) located at the upstream region of the second OPA enabled precise control of the temporal

DOI:10.1063/1674-0068/cjcp2104060

delay between the pump and probe laser pulses. The pump-probe time delays were scanned back and forth multiple times to minimize any small hysteresis effect, and the effects caused by the fluctuations and drifts in molecular beam intensity, laser pulse energy and pointing, *etc.* It was carefully checked that there were negligible *N*-ethylpyrrole clusters presented in the molecular beam.

The 2D photoelectron images were recorded at different pump-probe time delays and transferred to 3D distributions using the pBasex Abel inversion method [27]. The delay-dependent photoelectron 3D distributions were further integrated along the recoiling angle to derive the photoelectron kinetic energy distributions, *i.e.*, time-resolved photoelectron spectra (TRPES). Electron kinetic energy calibration was performed using multiphoton ionization of the Xe atoms. The cross-correlation (*i.e.*, instrumental response function (IRF)) between the pump and probe laser pulses was measured by the two-color (1+1′) non-resonant ionization of nitric oxide. The delay-dependent curves of the electron yield were fitted, based on the approximation that both the pump and probe laser pulses have a Gaussian profile. The derived (1+1′) IRFs were determined to be 150±15 fs (FWHM). This process also served to determine the time-zero which was checked before and after the TRPES measurements to make sure that there was no significant time-zero shift during the measurements.

III. RESULTS AND DISCUSSION

A. The UV absorption spectrum

The UV absorption spectrum of *N*-ethylpyrrole has not been previously reported. In this work, it was measured and is shown in FIG. 1. The main features are very similar to those of pyrrole and analogous assignments can be made. The weak, broad band which starts from ∼245 nm should be due to the transition to the $^1\pi\sigma^*$ states.

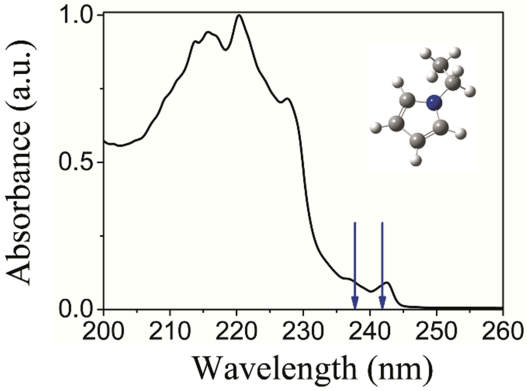

FIG. 1 The UV absorption spectrum of *N*-ethylpyrrole. The blue arrows indicate the pump wavelengths used in the current experiment.

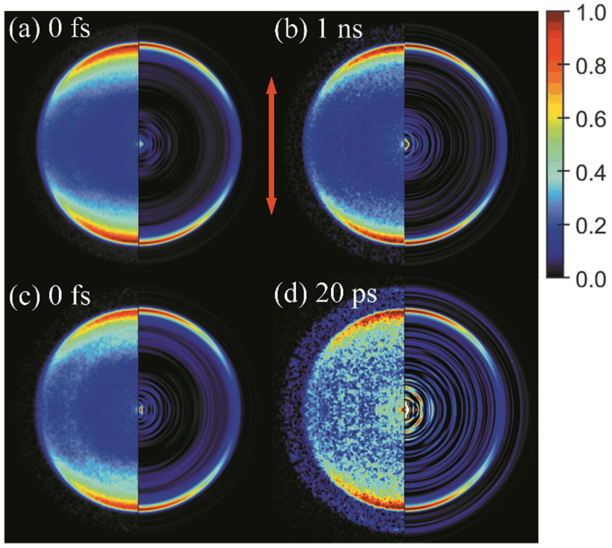

FIG. 2 (a, b) The two-color (1+1′) photoelectron images from *N*-ethylpyrrole at pump wavelength of 241.9 nm at selected pump-probe time delays, 0 fs and 1 ns, respectively. Time-invariant pump-alone and probe-alone photoelectron signals have been subtracted and the images are 4-fold symmetrised. The red double arrow indicates the polarization direction of pump and probe lasers. The left and right half images show the raw and deconvoluted ones, respectively. (c, d) Same as (a, b), but for 237.7 nm at 0 fs and 20 ps time delays, respectively.

B. The analysis of TRPES

The TRPEI method was employed for obtaining TRPES spectra of *N*-ethylpyrrole. The photoelectron images at pump wavelength of 241.9 nm at selected pump-probe time delays, 0 fs and 1 ns, are shown in FIG. 2 (a) and (b), respectively, with the left and right halves representing the raw and deconvoluted images. Note that time-invariant pump-alone and probe-alone photoelectron signals are regarded as the background photoelectrons and have been subtracted. Those images for 237.7 nm at 0 fs and 20 ps time delays are also shown in FIG. 2 (c) and (d), respectively. It is clear that the two-color (1+1′) photoelectron images show visible anisotropic distributions, with a relatively sharp ring feature (*i.e.*, the selected images presented in FIG. 2).

The TRPES spectra of *N*-ethylpyrrole at pump wavelengths of 241.9 and 237.7 nm after subtracting the

DOI:10.1063/1674-0068/cjcp2104060

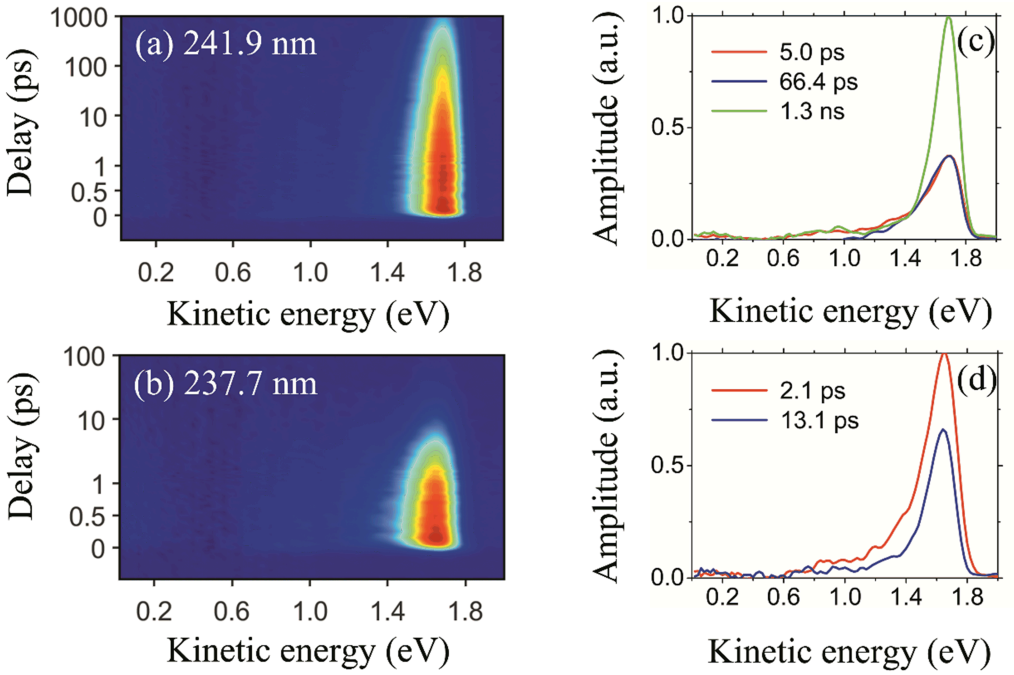

FIG. 3 (a, b) TRPES spectra of *N*-ethylpyrrole at pump wavelengths of 241.9 and 237.7 nm, respectively. The background photoelectrons generated from single-color multiphoton ionization have been subtracted. Note that a combination of linear and logarithmic scales is used in the ordinate. (c, d) The photoelectron kinetic energy dependent amplitudes of each component derived from a 2D global least-squares fit (see text) to the corresponding TRPES shown in (a, b).

background photoelectrons generated from single-color multiphoton ionization are shown in FIG. 3 (a) and (b), respectively. At these two pump wavelengths, the photoelectron spectra share large similarities, dominated by a single sharp and strong peak centred around the nearly same photoelectron kinetic energy. The time scale of the dynamics at pump wavelength of 241.9 nm is of the order of magnitude of 1000 ps, whereas that at 237.7 nm is around 10 ps. In order to extract more detailed information, a 2D global least-squares method was employed to simultaneously fit TRPES data at all time delays and photoelectron kinetic energies. The kinetic model used is expressed as the following equation:

$$S(\Delta t,\varepsilon_k)=\left[\sum_i A_i(\varepsilon_k)\cdot\exp\left(-\frac{\Delta t}{\tau_i}\right)\cdot H(\Delta t)\right]\otimes\mathrm{IRF} \quad (1)$$

Here, $S(\Delta t,\varepsilon_k)$ represents the 2D TRPES spectrum. Δt and ε_k are the pump-probe time delay and the kinetic energy of the emitted photoelectron, respectively. $A_i(\varepsilon_k)\cdot\exp(-\Delta t/\tau_i)$ is the contribution with lifetime τ_i and amplitude $A_i(\varepsilon_k)$. $H(\Delta t)$ is the unit step function. The corresponding IRF is experimentally measured independently. A satisfactory fit is achieved and lifetimes of 2.1±0.1 ps and 13.1±1.2 ps are derived at 237.7 nm. At 241.9 nm, one more time constant should be added and lifetimes of 5.0±0.7 ps, 66.4±15.6 ps and 1.3±0.1 ns are derived. The uncertainty of the time constant represents one standard deviation. In FIG. 3 (c) and (d), the partial photoionization cross sections of each component are also shown. The peak of 2.1±0.1 ps and 13.1±1.2 ps at 237.7 nm is 1.64±0.02 eV and that slightly shifts to 1.68±0.02 eV for 5.0±0.7 ps, 66.4±15.6 ps and 1.3±0.1 ns at 241.9 nm. A cut of the 2D global least-squares fit over the photoelectron kinetic energy range of 1.44−1.84 eV at pump wavelengths of 241.9 and 237.7 nm are shown in FIG. 4 (a) and (b), respectively. The contributions for each component derived from the least-squares fit are also included.

Here, excitation at 241.9 and 237.7 nm is suggested to only populate the $S_1(^1\pi\sigma^*)$ state of *N*-ethylpyrrole, which is the lowest singlet excited state lying above the ground state. All these extracted time constants are ascribed to the decay dynamics of the S_1 state, presumably vibrationally excited. It is well accepted that the S_1 state of pyrrole has 3s Rydberg state character at the FC region. This is the same as that of NMP [13, 17]. Such a 3s state may be expected to possess a minimum energy geometry very close to that of the ground state

DOI:10.1063/1674-0068/cjcp2104060

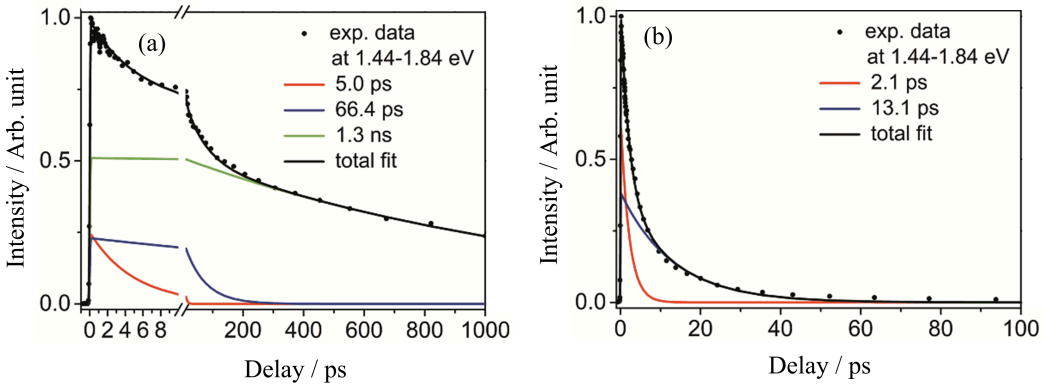

FIG. 4 (a) A cut of the 2D global least-squares fit over the photoelectron kinetic energy range of 1.44−1.84 eV at pump wavelength of 241.9 nm. The contributions for each component derived from the least-squares fit are also included. (b) Same as (a), but for 237.7 nm.

of the cation, resulting in the photoionization process being dominated by diagonal FC factors ($\Delta\nu$=0). This is consistent with the single sharp and strong peak observed in the TRPES spectra of *N*-ethylpyrrole.

C. The analysis of PADs

The time-resolved photoelectron angular distributions (TRPADs) can be derived by integrating the deconvoluted images over a desired kinetic energy range. Here the TRPADs at 241.9 and 237.7 nm are derived over a selected photoelectron kinetic energy range of 1.44−1.84 eV. These TRPADs are further analyzed in detail using the following expression for (1+1′) ionization with parallel linear polarizations [28, 29],

$$I(E,\Delta t,\theta) = \frac{\sigma(E,\Delta t)}{4\pi}[1+\beta_2(E,\Delta t)P_2(\cos\theta)+\beta_4(E,\Delta t)P_4(\cos\theta)] \quad (2)$$

Here, $\sigma(E,\Delta t)$ is the time-dependent electron kinetic energy distribution, $P_n(\cos\theta)$ terms are the nth-order Legendre polynomials, β_2 and β_4 are the well-known anisotropy parameters, and θ is the angle between polarization direction of the lasers and the recoil direction of photoelectrons. Satisfactory fits to PADs are achieved using Eq.(2) and the derived anisotropy parameters β_2 and β_4 for different time delays are also obtained. The derived β_2 and β_4 as a function of selected pump-probe time delays averaged over photoelectron kinetic energy range of 1.44−1.84 eV are plotted in FIG. 5 (a) and (b) for pump wavelengths of 241.9 and 237.7 nm, respectively.

The values of β_2 and β_4 are very similar for 241.9 and 237.7 nm pump wavelengths, consistent with the assignment that the initial excited electronic state at these two pump wavelengths should be the same. As mentioned above, we propose that the initial photoexcited states are the $S_1(^1\pi\sigma^*)$ vibrational states.

Based on the analysis of PADs, the S_1 state of *N*-ethylpyrrole is suggested to be dominated by the 3s Rydberg state character at the FC region with the following reasons: (i) At a first level of approximation (*i.e.*, atomic-like), single photon ionization of a pure 3s orbital should give rise to photoelectron partial waves of exclusively p character on the basis of angular momentum conservation (Δl=±1), leading to PADs peaking strongly along the laser polarization direction. The derived values of β_2 obtained from satisfactory fits to PADs are less than the limiting value of 2.0, with an average value of about 1.1. This is most possibly resulted from the somewhat mixed character of the 3s state, evidenced by a slight shift of the peak of the emitted photoelectron (1.64 eV at 237.7 nm and 1.68 eV at 241.9 nm). It was also previously found that there was vibronic mixing between the S_1 state and other higher lying states in NMP [13]. (ii) The derived value of β_2 is nearly invariant as pump-probe time delays, indicat-

DOI:10.1063/1674-0068/cjcp2104060

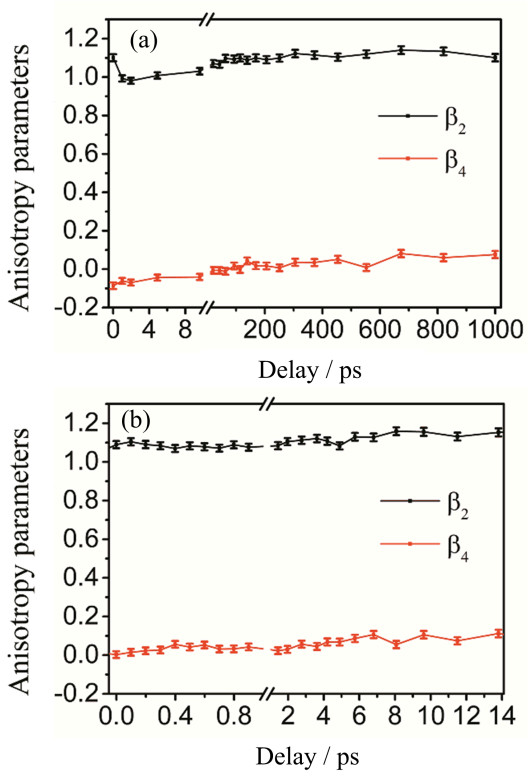

FIG. 5 (a) Anisotropy parameters, β_2 and β_4, as a function of selected pump-probe time delays averaged over photoelectron kinetic energy range of 1.44−1.84 eV at pump wavelength of 241.9 nm. The error bars represent one standard deviation derived from the fit of the PAD. (b) Same as (a), but for 237.7 nm.

ing that the excited electronic state involved at all time delays should be of the same with the s character. (iii) The derived value of β_4 to the overall PADs is around zero, strongly indicating that the PADs could be simply treated as one-photon ionization from the excited state, which means the one-photon absorption step from the ground state to the excited state is not involved with initial alignment, consistent with an isotropic orbital distribution of the 3s state.

D. The decay dynamics of the $S_1(^1\pi\sigma^*)$ state

As is well known, the pure $S_1 \leftarrow S_0$ transition is electric dipole forbidden in one-photon absorption for pyrrole. But this transition could have weak oscillator strength by vibronic mixing with allowed transitions to higher lying excited states, such as $^1\pi\pi^*$ states [22, 30]. In the case of *N*-ethylpyrrole, it should be weakly allowed due to the lowered symmetry (from C_{2v} to C_s) and enhanced by borrowing intensity from higher lying excited states, supported by the UV absorption spectrum shown in FIG. 1. Based on the analysis of experimental data, a reasonable decay mechanism of the $S_1(^1\pi\sigma^*)$ state of *N*-ethylpyrrole is proposed and discussed here. We conclude that excitation at both 241.9 and 237.7 nm results in population of the $S_1(^1\pi\sigma^*)$ state of *N*-ethylpyrrole with vibrational excitation. The lifetimes of a sub-picosecond and a few picoseconds are previously ascribed to intramolecular vibrational energy redistribution (IVR) process within the S_1 state of NMP [14, 16], while the relatively slow decaying component represents the depopulation rate of the S_1 state. Here we do not find any evidence to support that the lifetimes of 2.1±0.1 ps at 237.7 nm and 5.0±0.7 ps at 241.9 nm belong to IVR process. Especially for the 3s Rydberg state at the FC region, the IVR process is not expected to result in a significant varying of the photoionization cross-section before the wavepacket evolving out of the FC region. Therefore, by considering the broad bandwidth of the femtosecond pump laser pulse employed here and the different deactivation rates of the S_1 vibronic bands measured in NMP [16], we prefer to assign all the fitted time constants to the depopulation rates of different vibrational states in the $S_1(^1\pi\sigma^*)$ state of *N*-ethylpyrrole, followed by prompt $S_1 \rightarrow S_0$ internal conversion (IC) process with the lifetimes of 2.1±0.1 ps and 13.1±1.2 ps at 237.7 nm, 5.0±0.7 ps and 66.4±15.6 ps at 241.9 nm. However, the assignment of the lifetime of 1.3±0.1 ns at 241.9 nm is less clear-cut. The nanosecond component may be attributed to intersystem crossing (ISC) process to a lower lying $T_1(^3\pi\pi^*)$ state, which seems to be the decay channel for one vibrational state at 241.9 nm. This ISC process was also predicted for NMP in a previous study [14]. On the other hand, it also could be ascribed to IC to the ground state with a timescale of nanosecond to decay over a potential barrier along the N−C dissociation coordinate, while the lifetimes of 5.0±0.7 ps and 66.4±15.6 ps representing other vibrational states decaying fastly on the S_1 state potential energy surface. As the pump wavelength slightly decreases to 237.7 nm with increasing excitation, the corresponding TRPES spectrum clearly shows faster decay dynamics and the nanosecond component disappears, indicating that the decay channel of the S_1 vibrational states is a fast radiationless transition, $S_1 \rightarrow S_0$ internal conversion.

The proposed excited-state decay mechanism of the $S_1(^1\pi\sigma^*)$ state of *N*-ethylpyrrole is consistent with that clarified on the $S_1(^1\pi\sigma^*)$ state of NMP [13, 16]. The pr-

DOI:10.1063/1674-0068/cjcp2104060

esent experimental results highlight that the ethyl-substitution effects in N atom position is very similar to the methyl-substitution effects in NMP, resulting an increased barrier along the C−N dissociation coordinate. From a more general point of view, when the S_1 state is prepared with enough vibrational content, ISC process may compete with radiationless internal conversion relaxation through a conical intersection (CI) and become less important.

IV. CONCLUSION

The UV photoinduced dynamics of *N*-ethylpyrrole following excitation at pump wavelengths of 241.9 and 237.7 nm is investigated using the TRPEI method. Excitation at these two pump wavelengths results in population of the $S_1(^1\pi\sigma^*)$ vibrational states based on the detailed analysis of TRPES data and TRPADs. The lifetime of the $S_1(^1\pi\sigma^*)$ vibrational states is determined to be 5.0±0.7 ps, 66.4±15.6 ps, and 1.3±0.1 ns at 241.9 nm and it varies to 2.1±0.1 ps and 13.1±1.2 ps at 237.7 nm. The depopulation channel of the $S_1(^1\pi\sigma^*)$ vibrational states is suggested to be IC to the ground state, except for the vibrational state with a lifetime of 1.3±0.1 ns, which may decay followed by ISC to a lower lying triplet state.

V. ACKNOWLEDGMENTS

This work was supported by the National Natural Science Foundation of China (No.21833003 and No.21773213), the Strategic Priority Research Program of the Chinese Academy of Sciences (No.XDB17000000) and Chinese Academy of Sciences (GJJSTD20190002).

[1] G. M. Roberts and V. G. Stavros, Chem. Sci. **5**, 1698 (2014).
[2] R. Improta, F. Santoro, and L. Blancafort, Chem. Rev. **116**, 3540 (2016).
[3] L. A. Baker, B. Marchetti, T. N. V. Karsili, V. G. Stavros, and M. N. R. Ashfold, Chem. Soc. Rev. **46**, 3770 (2017).
[4] S. Soorkia, C. Jouvet, and G. Gregoire, Chem. Rev. **120**, 3296 (2020).
[5] V. Bhardwaj, D. Gumber, V. Abbot, S. Dhiman, and P. Sharma, RSC Adv. **5**, 15233 (2015).
[6] R. McDiarmid and X. Xing, J. Chem. Phys. **105**, 867 (1996).
[7] J. G. Philis, Chem. Phys. Lett. **353**, 84 (2002).
[8] N. Biswas, S. Wategaonkar, and J. G. Philis, Chem. Phys. **293**, 99 (2003).
[9] J. G. Philis, J. Mol. Spectrosc. **651**, 567 (2003).
[10] A. G. Sage, M. G. D. Nix, and M. N. R. Ashfold, Chem. Phys. **347**, 300 (2008).
[11] G. Piani, L. Rubio-Lago, M. A. Collier, T. N. Kitsopoulos, and M. Becucci, J. Phys. Chem. A **113**, 14554 (2009).
[12] C. M. Tseng, Y. T. Lee, and C. K. Ni, J. Phys. Chem. A **113**, 3881 (2009).
[13] G. Wu, S. P. Neville, O. Schalk, T. Sekikawa, M. N. R. Ashfold, G. A. Worth, and A. Stolow, J. Chem. Phys. **144**, 014309 (2016).
[14] L. Blancafort, V. Ovejas, R. Montero, M. Fernandez-Fernandez, and A. Longarte, J. Phys. Chem. Lett. **7**, 1231 (2016).
[15] T. Geng, O. Schalk, S. P. Neville, T. Hansson, and R. D. Thomas, J. Chem. Phys. **146**, 144307 (2017).
[16] K. C. Woo and S. K. Kim, Phys. Chem. Chem. Phys. **21**, 14387 (2019).
[17] A. R. Davies, D. J. Kemp, and T. G. Wright, Chem. Phys. Lett. **763**, 138227 (2021)
[18] A. L. Sobolewski and W. Domcke, Chem. Phys. **259**, 181 (2000).
[19] A. L. Sobolewski, W. Domcke, C. Dedonder-Lardeux, and C. Jouvet, Phys. Chem. Chem. Phys. **4**, 1093 (2002).
[20] R. Montero, A. Peralta Conde, V. Ovejas, M. Fernandez-Fernandez, F. Castano, J. R. Vazquez de Aldana, and A. Longarte, J. Chem. Phys. **137**, 064317 (2012).
[21] G. M. Roberts, C. A. Williams, H. Yu, A. S. Chatterley, J. D. Young, S. Ullrich, and V. G. Stavros, Faraday Discuss. **163**, 95 (2013).
[22] G. Wu, S. P. Neville, O. Schalk, T. Sekikawa, M. N. R. Ashfold, G. A. Worth, and A. Stolow, J. Chem. Phys. **142**, 074302 (2015).
[23] O. M. Kirkby, M. A. Parkes, S. P. Neville, G. A. Worth, and H. H. Fielding, Chem. Phys. Lett. **683**, 179 (2017).
[24] D. Yang, Z. Chen, Z. He, H. Wang, Y. Min, K. Yuan, D. Dai, G. Wu, and X. Yang, Phys. Chem. Chem. Phys. **19**, 29146 (2017).
[25] D. Yang, Y. Min, Z. Chen, Z. He, K. Yuan, D. Dai, X. Yang, and G. Wu, Phys. Chem. Chem. Phys. **20**, 15015 (2018).
[26] Z. G. He, Z. C. Chen, D. Y. Yang, D. X. Dai, G. R. Wu, and X. M. Yang, Chin. J. Chem. Phys. **30**, 247 (2017).
[27] G. A. Garcia, L. Nahon, and I. Powis, Rev. Sci. Instrum. **75**, 4989 (2004).
[28] K. L. Reid, Annu. Rev. Phys. Chem. **54**, 397 (2003).
[29] T. Suzuki, Annu. Rev. Phys. Chem. **57**, 555 (2006).
[30] S. P. Neville and G. A. Worth, J. Chem. Phys. **140**, 034317 (2014).

DOI:10.1063/1674-0068/cjcp2104060